Investigating Electronic Performance and Air-Stability of Carbohydrate-Bearing Semiconducting Polymers in Organic Field-Effect Transistors

*Madison Mooney,[1] Lauren Pandolfi,[1] Yunfei Wang,[2] Chenhui Zhu,[3] Garima Garg,[1] Ulrike Kraft,[4] Xiaodan Gu,[2] and Simon Rondeau-Gagné [1]**

[1] Department of Chemistry and Biochemistry, University of Windsor, Windsor, Ontario, Canada N9B 3P4

[2] School of Polymer Science and Engineering, The University of Southern Mississippi, Hattiesburg, MS 39406, USA

[3] Advanced Light Source, Lawrence Berkeley National Laboratory, Berkeley, CA 94720, USA

[4] Organic Bioelectronics Research Group, Max Planck Institute for Polymer Research, 55182 Mainz, Germany

Keywords:

ABSTRACT

INTRODUCTION

Research in organic semiconductors plays a crucial role in the development of next-generation electronics as emerging electronics require enhanced versatility and tuneability to interact in original ways with the human body and the environment.[1–3] The development of electronic devices with applications in personalized healthcare, energy production, and smart packaging rely not only on high-performance materials, but also the enabling of innovative properties such as molecular flexibility, improved mechanical endurance, and biocompatibility.[4–7] Semiconducting polymers (SPs) have a strong potential for use in next-generation electronics due to their solution processability and synthetic tuneability.[8,9] Previous advancements in this field have unveiled SPs with self-healing properties, high charge mobilities, and intrinsic stretchability for direct application in a wide variety of applications.[10–13] Properties such as solvent resistance,

thermochromism or solvatochromism have further diversified the applicability of SPs in sensors and diagnostic technologies.[14–18] Despite these many exciting developments, commercialization of next-generation organic electronics remains a challenge. Industrial scale-up, batch-to-batch variation and stability in environmental conditions are all key challenges that often need to be addressed for the commercialization of organic electronic devices.[19,20] Investigating structure-processing-property relationships is, thus, necessary to bridge the gap to commercialization of high-performance SPs and expend the use of these emerging devices in various fields.

A deeper understanding of the relationship between material structure, processing, and device properties is critical for the development of next-generation organic electronics. Manipulation of structure-property relationships has led to the design and preparation of high-performance SPs with charge mobilities in organic field-effect transistors (OFETs) often surpassing 10 cm^2/Vs.[21,22] In π-conjugated SPs, chemical design strategies such as side chain engineering or backbone modification have been shown to have significant and predictable impacts on device performance properties.[23–25] However, processing conditions, i.e. the experimental conditions used to process the active materials in the functional devices, can also substantially influence the electronic performance and device properties by directly impacting thin film morphology and interlayer compatibility.[26,27] Therefore, as highlighted often in the literature, it is imperative to consider not only structure-property relationships in the design of a new semiconducting materials, but also the impact of synthetic design on processing parameters.[20] For example, Di *et al.* used a solvent-assisted reannealing post-treatment to improve molecular packing of several SPs, resulting in a 3-fold improvement of charge mobility in OFETs.[28] Chaudhary and colleagues also showed that, by simply modifying solvent selection and using an off-centered spin coating technique, a 50-fold increase in charge mobility could be achieved for P3HT which was

attributed to the generation of highly ordered crystalline nanowires.[29] These approaches, among many others, demonstrate that the investigation of structure-processing-property relationships is crucial to the development of high-performance materials.

Previously, we synthesized a series of isoindigo-based SPs with carbohydrate side chains to improve processability in eco-friendly solvents.[30] By varying the ratio of carbohydrate-bearing block in a statistical random copolymer (from 10 to 50 mol%), we were able to tune the solubility of the polymers and achieve processability in a *n*-butanol/*o*-anisole solvent blend, a greener alternative to typically-used halogenated solvents. The materials were directly investigated in OFETs to evaluate the greener processing conditions and their impact on device characteristics. We found that the performance of the carbohydrate-containing polymers was comparable to that of a reference polymer bearing only branched alkyl side chains. Furthermore, electronic performance was maintained in devices processed from the green solvent blend. In a later study, we found that, by increasing the ratio of carbohydrate-bearing block (80 and 100 mol%) and using a more rigid donor monomer, triggered solvent-resistance could be achieved through intermolecular hydrogen bonding of the carbohydrate side chains.[31] OFETs fabricated from these polymers using *o*-anisole showed no loss of performance, and good film quality was observed after solvent-resistance had been triggered or after subsequent submersion in a variety of solvents. Overall, while these polymers possess exciting properties for the green processing of semiconducting polymers and triggered solvent-resistance for additive manufacturing of organic electronics, they demonstrated relatively low charge mobilities in OFETs, presenting a critical barrier to their expansion and application in functional devices.

This work overcomes that barrier by probing the structure-processing-property relationships of a new series of carbohydrate-bearing SPs. Additionally, investigation of the

environmental stability of these polymers in OFETs was undertaken to evaluate this critical property for broad application and future commercialization of related technologies. Adapting previously reported synthetic procedures, we report the synthesis and characterization of a series of isoindigo-based SPs that exhibit significantly improved electronic performance by varying several key structural and processing parameters. In particular, the length of the galactose-terminated side chain was modified to investigate the impact on solid-state properties and charge transport.[24,32] The monomers were also copolymerized with a bithiophene donor unit.[33] Upon structural characterization of the new polymer series, electronic performance was investigated in OFETs. A meticulous structural characterization of the new polymer series was performed using atomic force microscopy (AFM) and grazing incidence wide-angle x-ray scattering (GIWAXS) to evaluate the solid-state properties of the new materials. These findings were then closely correlated to electronic performance, probed through the fabrication of OFETs. Important structure-property relationships and trends were established through this comparison and processing-property relationships were also explored through variation in device annealing and determination of device stability upon exposure to air. Oxygen-doping effects observed after prolonged exposure to air were also investigated using contact resistance measurements. Using eco-friendly materials such as carbohydrates and bio-inspired isoindigo, this new series of polymers demonstrates significantly improved electronic performance and air stability, both critical to commercialization of the next generation of organic electronics. This work serves as a model for the investigation of structure-processing-property relationships and the importance of these relationships to the optimization of electronic performance in SPs.

RESULTS AND DISCUSSION

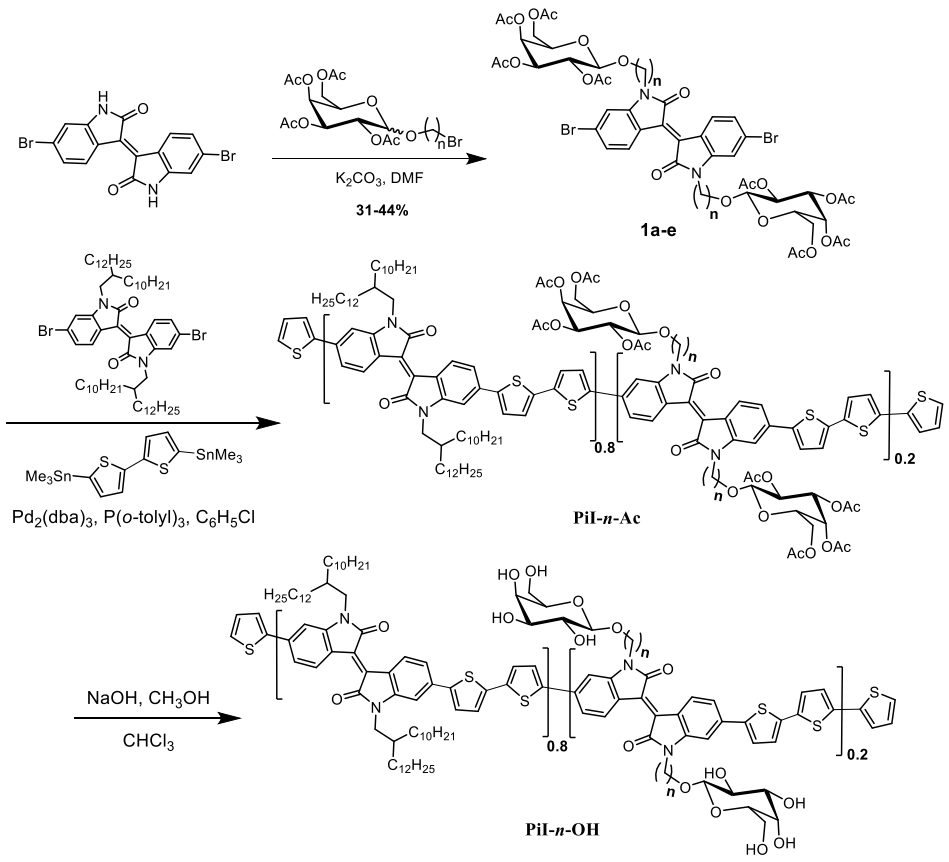

Scheme 1. *Synthetic pathway for the preparation of semiconducting polymers* **PiI-*n*-Ac** *and* **PiI-*n*-OH**.

The synthetic route to the isoindigo-bithiophene statistical random copolymers, **PiI-*n*-Ac** and **PiI-*n*-OH**, is depicted in Scheme 1, with ***n*** referring to the number of carbons in the carbohydrate-containing side-chain spacer unit. A detailed experimental procedure for the synthesis of polymers **PiI-*n*-Ac** and **PiI-*n*-OH** is described in Supporting Information. Briefly, bromine-terminated alcohols with alkyl spacer chain lengths n = 4, 6, 8, 10, 12 carbons were reacted with β-D-galactose pentaacetate in the presence of boron trifluoride diethyl etherate. The crude side chains were then reacted directly with 6,6'-dibromoisoindigo to afford monomers **1a-e**

in good yields (31 - 44 %). Although synthetic procedures to access these polymers were previously published,[30,31] the synthetic approach was revisited to improve the synthetic versatility (critical for expanding this approach to other saccharide units), to reduce side-product formation, and achieve overall higher yields. Notably, previous synthetic approaches often led to O-alkylation and other side-product formation that reduced synthetic yields and complicated purification. To address this synthetic challenge, the alkylation of the isoindigo core with pre-functionalized side chains bearing galactose units was performed, which allowed for increased yields by preventing potential O-alkylation and for simpler purification. Upon obtention of the different carbohydrate-containing monomers, statistical random copolymerization was performed *via* Stille cross-coupling with monomers **1a-e** (20 mol%), (E)-6,6′-dibromo-1,1′-bis(2-decyltetradecyl)-[3,3′-biindolinylidene]-2,2′-dione (80 mol %) and 5,5'-bis(trimethylstannyl)-2,2'-bithiophene to afford acetyl-protected random copolymers **PiI-*n*-Ac**. Polymers **PiI-*n*-OH** were attained by removing the acetyl protecting groups according to previously reported basic conditions.[30]

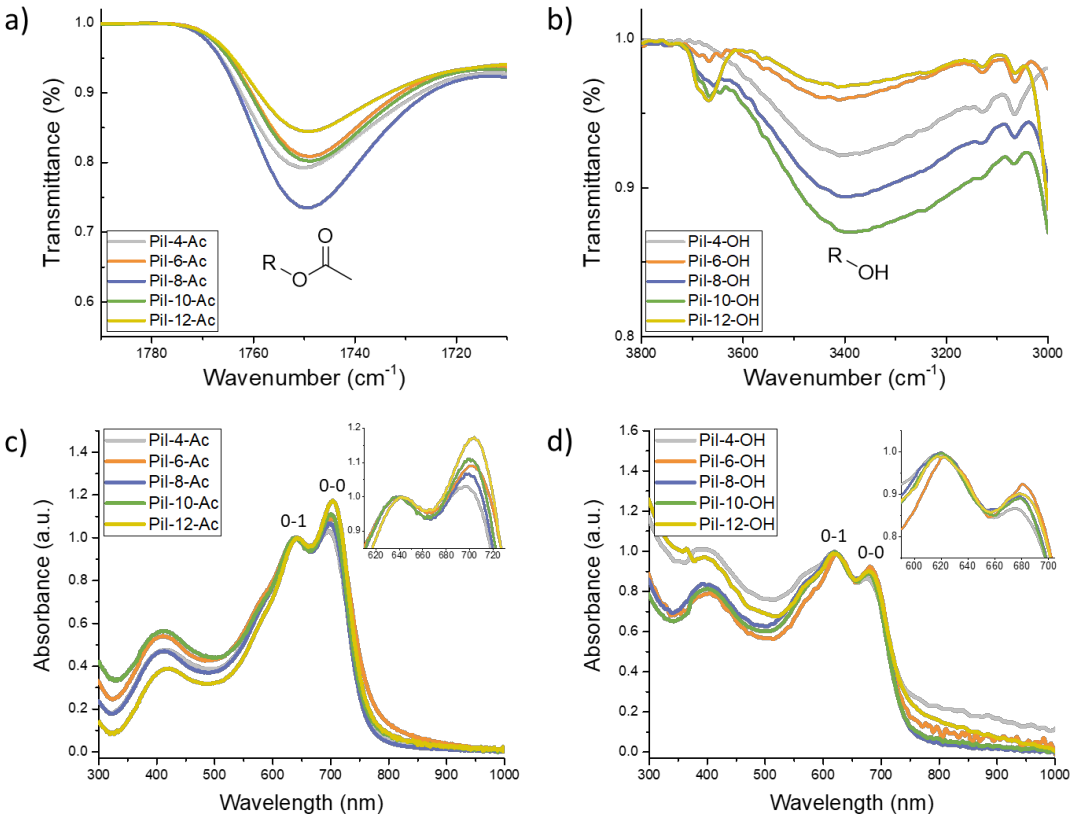

Figure 1. Characterization of the new polymers before and after deprotection. Fourier-transform infrared (FTIR) spectra of galactose-bearing polymers showing a) carbonyl and b) alcohol stretching peaks. Normalized UV-vis spectra of c) the **PiI-*n*-Ac** polymer series and d) the **PiI-*n*-OH** polymer series showing vibrational peaks 0-0 and 0-1.

Structural characterization of **1a-e** was carried out by ^{1}H NMR, ^{13}C NMR and high-resolution mass spectrometry (see Supporting Information). Because the polymer series was generated through a random copolymerization method, the experimental ratios of the galactose-bearing monomer within the polymers were confirmed by ^{1}H NMR at 120 °C in 1,1,2,2-tetrachloroethane-d_2, as shown in Figure S1. A comparison of a chemical shift associated with the anomeric position of the carbohydrate unit (δ = 4.2 ppm) and the chemical shift associated with the isoindigo lactam ring (δ = 3.8 ppm) confirms that all polymers are composed of approximately

20% galactose-bearing isoindigo units. Furthermore, acetyl-deprotection to obtain **PiI-*n*-OH** was confirmed by Fourier-transform infrared (FTIR) spectroscopy. As shown in Figure 1 and Figure S2, deprotection of the alcohol moieties is confirmed by loss of a C=O stretching peak at 1750 cm^{-1} [1] associated with the acetyl protecting groups and the appearance of a broad O-H stretching band at 3370 cm^{-1}. Upon structural confirmation, the **PiI-*n*-Ac** and **PiI-*n*-OH** polymer series were further characterized by various methods, and the results are summarized in Table 1.

Table 1. *Structural and optoelectronic characterization of the new isoindigo-based polymers. Measured molecular weights, polydispersity, optical properties, energy levels and thermal stability.*

	M_n (kDa)[a]	M_w (kDa)[a]	$Đ_w$[b]	$\lambda_{max\ (film)}$ (nm)[c]	E_g^{opt} (eV)[d]	HOMO (eV)[e]	LUMO (eV)[f]	T_d (°C)[g]
PiI-4-Ac	14.1	18.0	1.3	696	1.58			374
PiI-4-OH				683	1.59			375
PiI-6-Ac	21.9	35.8	1.6	700	1.56			377
PiI-6-OH				686	1.60			378
PiI-8-Ac	24.1	39.7	1.6	698	1.59			385
PiI-8-OH				685	1.61			381
PiI-10-Ac	22.0	38.1	1.7	700	1.57			386
PiI-10-OH				686	1.61			387
PiI-12-Ac	26.0	45.5	1.8	703	1.57			385
PiI-12-OH				684	1.59			386

[a] Number-average molecular weight and weight-average molecular weight estimated by high temperature SEC in 1,2,4-trichlorobenzene at 180 °C using polystyrene as standard. [b] Dispersity defined as M_w/M_n. [c] Absorption maxima in thin film. [d] Calculated by the following equation: gap = $1240/\lambda_{onset}$ of polymer film. [e] Calculated from cyclic voltammetry (Potentials vs. Ag/AgCl) using 0.1 M $TBAPF_6$ in CH_3CN as electrolyte where E_{HOMO} = -4.38 eV - (Ox_{Onset}). [f] Estimated from calculated E_g and HOMO. [g] Estimated from TGA at 5% mass loss.

High-temperature size-exclusion chromatography was used to determine the molecular weight and polydispersity of the polymers. While most polymers were found to have similar molecular weights (around 20 kDa), **PiI-4-Ac** is slightly lower at 14kDa. This is attributed to a decrease in solubility of both the monomer and resulting polymer arising from the short spacer chain between the isoindigo core and bulky carbohydrate end-group. Optical bandgap and λ_{max} of all polymers were determined using UV-Vis spectroscopy (Figure S3). As shown in Table 1, the bandgaps are comparable for all polymers, indicating that the length of the side-chain spacer unit and polarity of the carbohydrate end-group do not significantly impact the electronic properties of the resulting polymers. The thermal stability of the polymers was also assessed by thermogravimetric analysis (TGA). As shown in Table 1 and Figure S5, thermal decomposition was measured for each polymer at 5% mass loss. All polymers had sufficiently high thermal stability at $T_d > 350$ °C.

The optical properties of the **PiI-*n*-Ac** and **PiI-*n*-OH** polymers were further characterized by thin-film UV-Vis spectroscopy. As shown in Figures 1 and Figure S3, a broad absorption band attributed to donor-acceptor charge transfer in the polymer backbone can be observed centered at approximately $\lambda = 680$ nm. Comparison of the two vibrational peaks (0-0 and 0-1) of the absorption band gives insight to the solid-state aggregation behaviour of the polymers.[34] As expected, the length of the side chain spacer has little impact on λ_{max} (associated to the effective conjugation length), but was found to impact solid-state aggregation. As noted in Figure 1c, aggregation increases with increasing side chain spacer length. The shorter chains and relatively bulky galactose end-groups can disrupt polymer chain interdigitation and aggregation compared to the longer chains, which allow for greater flexibility and closer packing of the polymer backbones. Additionally, a decrease in aggregation is observed in the **PiI-*n*-OH** series compared to the **PiI-*n*-**

Ac series. This has been previously observed in conjugated polymers with hydrogen bonding side chains and indicates that the formation of intermolecular hydrogen bonding reduces aggregate formation by disrupting the stacking of polymer chains.[35]

Following material characterizations, these polymers were evaluated in OFETs. The full experimental procedure for the fabrication of the devices can be found in the Supporting Information. Briefly, devices with bottom-gate top contact configuration were prepared by spin-coating solutions of 5 mg/mL in 1,1,2,2-tetrachloroethane onto octyltrimethoxysilane (OTS) functionalized Si/SiO_2.[36] Physical vapour deposition was then used to deposit gold electrodes of various channel lengths and widths. Figures S6 to S9 show the measured output and transfer curves of the **PiI-*n*-Ac** and **PiI-*n*-OH** polymer series, with key results summarized in Table S1. Linear fitting of $I_{DS}^{1/2}$ *vs.* V_{GS} from the transfer curves in the saturation regime was used to extract charge carrier mobility (μ_{sat}) using the following equation: $I_{DS\,(sat)} = (WC/2L)\ \mu_{sat}\ (V_G - V_{th})^2$, where I_{DS} is drain current, W and L are channel width and length, C is the dielectric constant of SiO_2, V_G is gate voltage and V_{th} is threshold voltage.

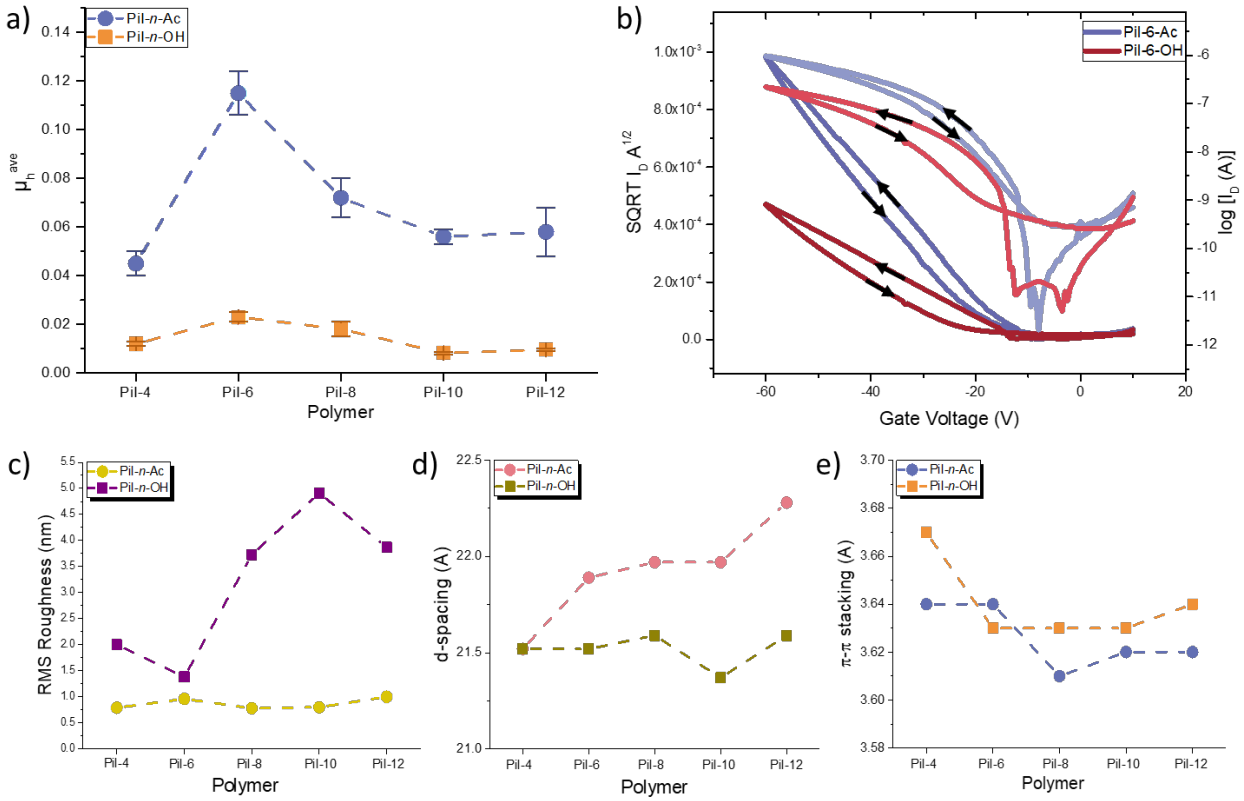

Figure 2. OFET characteristics of the new isoindigo-based polymers. a) Average hole mobilities of polymers **PiI-*n*-Ac** and **PiI-*n*-OH** with b) transfer curves of **PiI-6-Ac** and **PiI-6-OH** showing hysteresis behaviour. Trends in c) RMS roughness measured by AFM, and d) d-spacing and e) in-plane π-π stacking measured from GIWAXS.

As shown in Figure 2a and Table S1, the mobilities measured for all polymers were similar, with the majority falling within the range of 10^{-2} cm^2/Vs. While these results are not among the highest reported performances, comparable values have previously been published for similarly side chain engineered isoindigo-based polymers.[37,38] Importantly, all devices showed dramatically improved charge mobilities compared to our previous work. Previously, we synthesized isoindigo-based polymers bearing galactose side chains with two key structural differences: (1) a nine-carbon length side chain spacer between the isoindigo core and carbohydrate end-group was used and (2)

the isoindigo monomers were copolymerized with a thiophene donor.[30] When tested in OFETs, the highest average mobility of these polymers was found to be 2.3 x 10^{-4} cm^2/Vs, significantly lower than the highest performance recorded in this work, 0.115 cm^2/Vs (Table S1). By using a more electron rich donor, bithiophene, and even-numbered carbon spacer chains to exploit the well-documented odd-even effects,[24,39] we improved the electronic performance of carbohydrate-containing SPs by up to three orders of magnitude.

Within each of the new polymer series, **PiI-6-Ac** and **PiI-6-OH** demonstrated the highest mobilities, with average values of 0.115 cm^2/Vs and 0.023 cm^2/Vs respectively. The poorest performing polymers from each series were **PiI-4-Ac** (0.045 cm^2/Vs) and **PiI-10-OH** (0.008 cm^2/Vs). As shown in Figure 2a, the protected **PiI-*n*-Ac** polymers exhibit higher mobilities than the deprotected **PiI-*n*-OH** series by an average of 5-fold. This is consistent with previous findings from our group and can be in part attributed to the charge trapping sites generated by the exposure of the polar alcohol groups on the carbohydrate units of the **PiI-*n*-OH** series.[31,40,41] This charge trapping can also be observed through the increased hysteresis behaviour in the transfer curves of the **PiI-*n*-OH** series compared to the **PiI-*n*-Ac** polymers (Figures 2b, S7 and S9). The **PiI-*n*-Ac** series also showed higher on/off current ratios and lower threshold voltages compared to the **PiI-*n*-OH** series.

To gain insight on thin-film morphologies and their impact on device characteristics, solid-state characterizations were performed with AFM and GIWAXS, with the results summarized in Table S2. AFM was used to investigate the surface microstructures and determine the root-mean-square (RMS) roughness of the polymer films. Height and phase images are shown in Figures S10 and S11. As shown in Figure 2c, the **PiI-*n*-Ac** series form smoother films than the **PiI-*n*-OH** polymers, with an average root-mean square (RMS) roughness of 0.87 nm for the **PiI-*n*-Ac** series

compared to a much greater average value of 3.18 nm for the **PiI-*n*-OH** series. The increased roughness of the **PiI-*n*-OH** polymers can be attributed to a decrease in solubility resulting from hydrogen bonding between the carbohydrate side chains. The RMS roughness of the **PiI-*n*-Ac** series compared to that of the **PiI-*n*-OH** polymers is inversely related to the observed charge carrier mobilities, indicating that the smoother films yielded better-performing devices. Among the **PiI-*n*-OH** series, **PiI-6-OH** possesses the lowest RMS roughness, 1.38 nm, again correlating with the higher charge carrier mobility observed compared to the rest of the series. Among all devices, **PiI-10-OH** and **PiI-12-OH** show the highest RMS roughness (4.91 nm and 3.87 nm respectively) and lowest charge mobilities (0.008 cm^2/Vs and 0.009 cm^2/Vs respectively), further correlating film roughness with electronic performance. Since the RMS roughness was similar for all **PiI-*n*-Ac** polymers, ranging from 0.78 nm to 1.00 nm, surface morphology likely did not play a significant role in influencing electronic performance.

GIWAXS was used to further investigate the effects of molecular packing on the electronic performance of these polymers. 2D scattering patterns and 1D sector-averaged profiles are shown in Figures S12 to S14. The *d*-spacing of the side chains from (100) peak and π-π stacking of the backbones from (010) peak of the polymers in thin films were determined and summarized in Table S2. As shown in Figure 2d, *d*-spacing for the **PiI-*n*-OH** series was found to be closer than that of the **PiI-*n*-Ac** series, with average distances of 21.52 Å and 21.93 Å for each series respectively. This is consistent with our previous works and indicates that the hydrogen bonding between the exposed alcohol groups of the carbohydrate units leads to closer packing of the side chains.[31] Interestingly, side chain length does not appear to have significant impact on d-spacing in the **PiI-*n*-OH** series. Conversely, when the alcohol units are not exposed in the **PiI-*n*-Ac** series, spacer chain length bears a more substantial impact on d-spacing, with increasing chain length

more closely correlated to greater spacing between side chains due to the bulky carbohydrate end-groups and an absence of hydrogen bonding to draw them together (Figure 2d). When compared to our previous work, the odd-even effect can be seen by the closer packing of these polymer side chains. In our previous work using an odd numbered spacer chain ($n = 9$), we observed a d-spacing of 24.17 Å. This distance is significantly larger than any of the polymers in this work, whose largest d-spacing distances ranged from 21.37 Å to 22.28 Å.[30] Furthermore, no higher order reflections were observed for the previous works, while both (200) and (300) reflections were observed for nearly all of the **PiI-*n*-Ac** series and several of the **PiI-*n*-OH** series (Figures S12 and S13), indicating that the changes in polymer backbone structure and side chain spacer in this work significantly improve long range order in solid-state. Notably, these polymers all showed π-π stacking in only the in-plane direction (Figures S12 to S14), signifying that the polymer chains pack in an edge-on orientation relative to the substrate, which has been reported to be more favourable compared to face-on orientation for electronic performance in OFETs.[42]

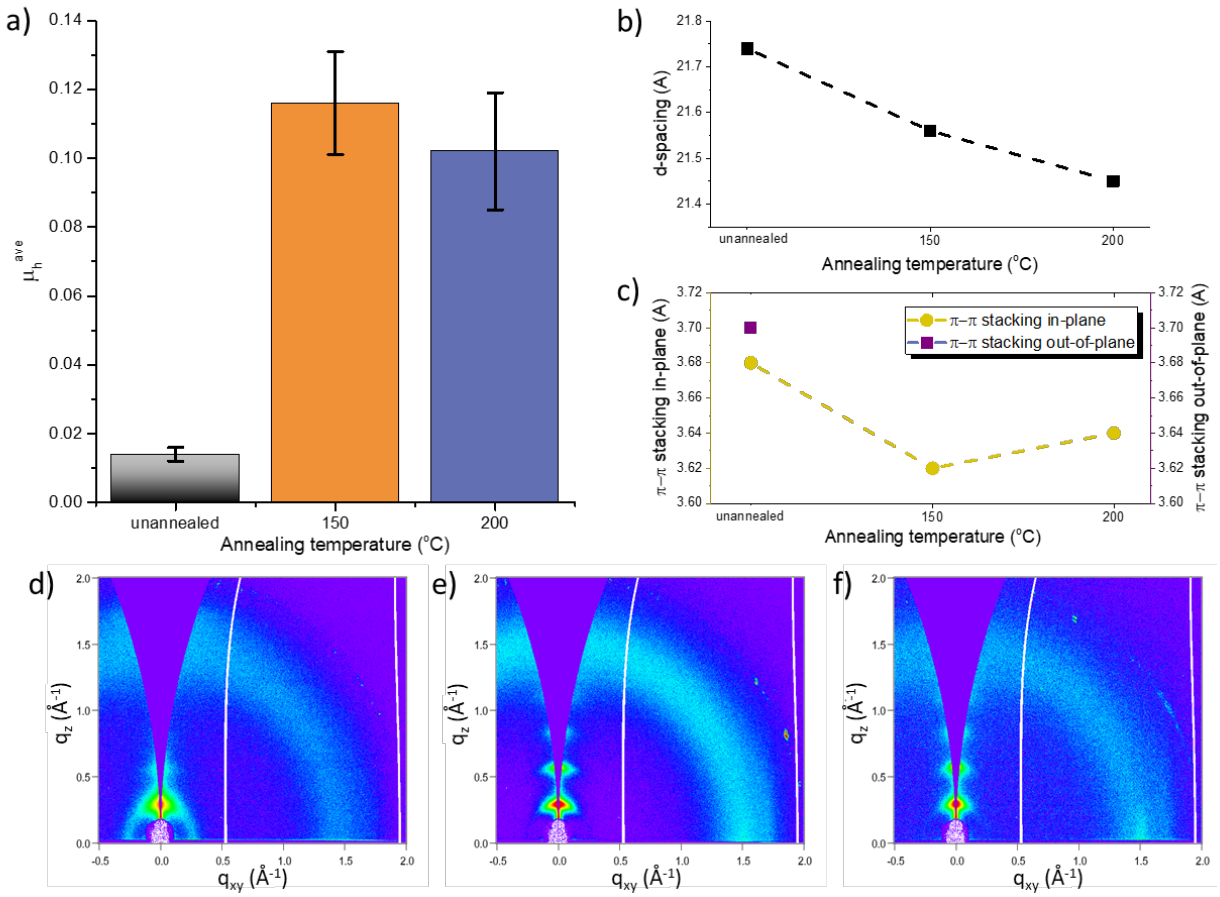

Figure 3. OFET characteristics of **PiI-6-Ac** under varied annealing conditions. a) Average hole mobilities, b) d-spacing, and c) π-π stacking of **PiI-6-Ac** after annealing at various temperatures. 2D scattering patterns of **PiI-6-Ac** d) unannealed, e) annealed at 150°C, and f) annealed at 200°C.

To probe the effects of annealing on electronic performance, **PiI-6-Ac** was chosen to fabricate OFETs annealed at several different temperatures. The output and transfer characteristics are shown in **Figures S15** to **S16**, with the results summarized in Table S3. Thin films were annealed at 150 °C and 200 °C for 30 minutes each to determine whether variation in annealing temperature plays a significant role in the improvement of electronic performance. An unannealed device was also tested to determine how annealing impacts the performance and morphology of the polymer. Interestingly, it was found that annealing temperature does not play a significant role

in electronic performance, with similar charge mobilities measured at both annealing temperatures. The average values obtained for devices annealed at 150 ˚C (0.116 cm^2/Vs) and 200 ˚C (0.102 cm^2/Vs) were found to be within each other's standard deviations, and within that of the initial **PiI-6-Ac** device (0.115 cm^2/Vs), which was annealed at 175 °C for 30 minutes. As shown in Figure 3a, these values were significantly higher than the charge mobility of the unannealed device, which showed an average charge mobility of only 0.014 cm^2/Vs, a full order of magnitude lower than the annealed devices. The substantial improvement in charge mobility measured after annealing can be directly correlated to changes in molecular packing, observed through GIWAXS. 2D scattering patterns are shown in Figure 3d-f, with 1D sector-averaged profiles and calculated values in Table S4 and Figure S17. As shown in Figure 3b-c, thermal annealing bears a small but positive effect on d-spacing and π-π stacking, with slightly closer packing of both side chains and polymer backbones observed after annealing. Notably, the impact of annealing on long range order and packing orientation is much more significant. The unannealed film lacks a (300) reflection compared to the annealed samples and exhibits both in-plane and out-of-plane π-π stacking. Upon annealing, the samples show improved long-range order and a transition to fully edge-on orientation relative to the substrate rather than a mix of edge and face-on, which is less favourable for charge transport. The increase in long range order and reorientation of the polymer chains to solely edge-on packing support the significant increase in charge mobility measured after annealing the devices.

An important consideration for expanding the application of organic electronics is stability in environmental conditions in which the device may be used. SPs often exhibit poor stability when exposed to oxygen and moisture.[8,43] For this reason, the majority of reported charge mobilities are measured in controlled environments from devices fabricated in air-free conditions. To investigate

the air stability of the **PiI-*n*-Ac** and **PiI-*n*-OH** polymer series, OFETs were fabricated and tested after exposure to ambient conditions for various lengths of time. The fabrication of these devices was conducted in completely air-free conditions in an N_2-filled glovebox. This is in contrast to the previously discussed results, where the solution preparation and spin-coating steps of device fabrication were conducted in open-air conditions. By fabricating the devices in a completely air-free environment, a baseline could be established to determine the effects of air exposure over time. For each polymer, devices were tested on the same substrate in pristine (air-free) conditions, then after successive exposure to ambient air for 24 hours, 72 hours and 10 days (240 hours). The transfer characteristics of these devices are shown in Figures S18 and S19 with the results summarized in Table S5.

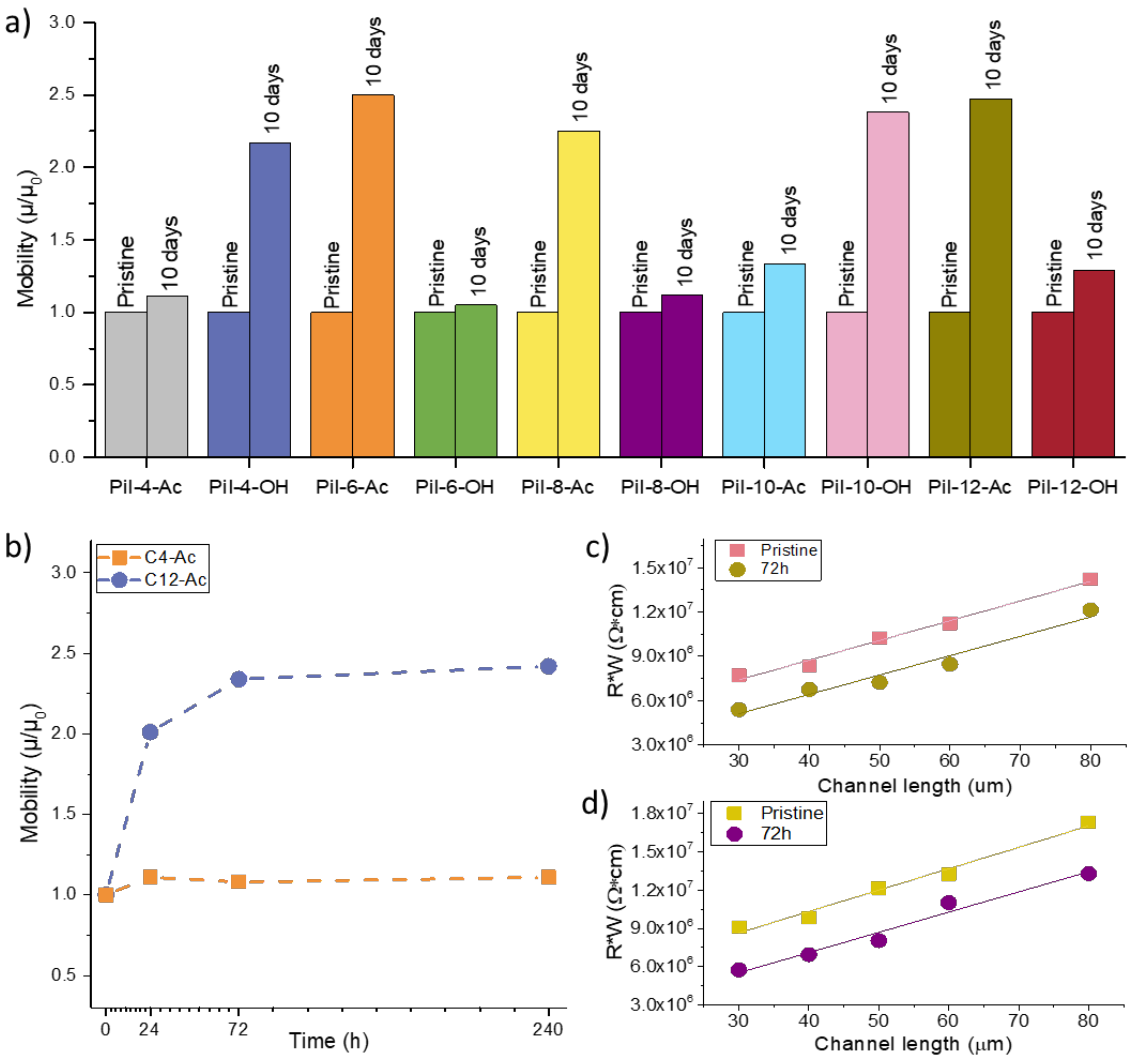

Figure 4. OFET characteristics of the new isoindigo-based polymers upon exposure to air. a) Charge carrier mobilities (extracted from the transfer characteristics in the saturation regime) in air-free (pristine) conditions, then after exposure to air for 10 days, normalized to $\mu_{pristine} = 1$. b) Normalized change in charge mobility over time for **PiI-4-Ac** and **PiI-12-Ac**. Width-normalized resistance (R*W) of polymers c) **PiI-4-Ac** and d) **PiI-12-Ac** calculated from devices of various channel lengths. Line-of-best-fit used to calculate the width-normalized contact resistance.

As shown in Figure 4a, these polymers all possess excellent air stability, with no degradation of charge mobility after 10 days of exposure to ambient air. Surprisingly, the charge carrier mobilities improved after prolonged exposure to air by as much as 2.5 times that of the pristine values. Additionally, the transfer curves demonstrate more ideal behaviour after exposure to air. As shown in Figure S18 and S19, the square-root curves become more linear with increasing exposure to air. Interestingly, similar observations of increased charge mobility and device stability upon exposure to air over time were reported with an indacenodithiophene-co-benzothiadiazole polymer, in which these effects were attributed to oxygen diffusion and doping.[44] Incidental exposure to oxygen in air is known to p-dope some organic semiconductors through various charge transfer mechanisms.[45–49] The significant improvement of measured charge mobilities observed in these devices after exposure to air can therefore be attributed to incidental oxygen-doping effects.

To investigate the increase in OFET performance observed after exposure to air, the width-normalized contact resistance (R_cW) was determined in pristine (air-free) devices, then after exposure to air for 72 hours for two representative polymers. Contact resistance can be affected by doping effects through improvement of charge injection at the metal-semiconductor interface.[45,50] Therefore, changes observed in contact resistance after exposure to air can be correlated to doping effects caused by exposure to air. Since all polymers show similar trends of increasing performance over time, **PiI-4-Ac** and **PiI-12-Ac**, polymers at each extreme of the series, were chosen for this experiment.

Width-normalized contact resistance was calculated for devices from polymers **PiI-4-Ac** and **PiI-12-Ac** in pristine conditions and after exposure to air for 72 hours using the transmission line method (TLM) according to previous reports.[50–53] This method is based on the assumption

that, in the linear regime, the total resistance of a transistor is the sum of the channel resistance and the contact resistance. As shown in Figure 4c and d, by plotting the width-normalized resistance against channel lengths ranging from 30 to 80 μm, the total resistance can be extrapolated to a channel length of 0, effectively eliminating contributions of channel resistance to total resistance. In other words, the total resistance at a channel length of 0 is an estimate of the contact resistance. What remains can be considered an estimate of contact resistance. Total resistance (R) for each device was calculated using the drain current (I_D) at a set overdrive voltage (V_{GS} - V_{th} = -20V) and a fixed drain voltage (V_{DS} = -5V), then normalized by channel width (W) according to the following equation: $R*W = (I_D / V_{DS}) W$. As shown in Figure 4 and Table S6, the contact resistance decreases significantly upon exposure to air for both the **PiI-4-Ac** and **PiI-12-Ac** devices by approximately 3-fold (from 3.61 x 10^6 Ω•cm to 0.82 x 10^6 Ω•cm and 3.41 x 10^6 Ω•cm to 1.14 x 10^6 Ω•cm respectively), in agreement with the observed increases in charge mobilities after prolonged exposure to air. This result supports the conclusion that the increased performance of these devices observed after prolonged exposure to air is the result of incidental oxygen-doping. Additionally, when comparing **PiI-4-Ac** to **PiI-12-Ac**, the contact resistance values are very similar, indicating that the side chain structure has a negligible effect on the resistance and oxygen doping effects of the devices.

CONCLUSION

In summary, we have developed two series of isoindigo-based polymers with galactose side chains containing varied alkyl spacer lengths (**PiI-*n*-Ac** and **PiI-*n*-OH**) to investigate structure-processing-property relationships toward the enhancement of electronic performance. Upon structural characterization, these polymers were used as active layers in OFETs to determine

their electronic properties. Compared to our previous works, these polymers exhibited dramatically improved charge mobilities by up to three orders of magnitude. Investigation of thin film characteristics revealed that the **PiI-n-OH** series displays closer d-spacing than the **PiI-*n*-Ac** series, resulting from hydrogen bonding. However, the **PiI-*n*-OH** series also show greater film roughness and poorer electronic performance compared to the **PiI-*n*-Ac** series. By contrast, the **PiI-*n*-Ac** series had smoother films and closer π-π stacking, accounting for the observed increase in charge mobility. Both series exhibit favourable edge-on orientation of the polymer backbones long-range order, observed by GIWAXS. Interestingly, though thermal annealing temperature had little effect on device performance, annealing was crucial to achieve favourable orientation and long-range order, leading to an increase in charge mobility by an order of magnitude compared to unannealed devices. These polymers all demonstrated excellent stability upon exposure to ambient air for 10 days and showed substantial improvement of electronic performance by up to 2.5 times, resulting from incidental oxygen doping. The doping effects were correlated to a reduction in contact resistance by approximately 3-fold in devices after exposure to air. This work presents an important model for the investigation and optimization of electronic performance in sidechain engineered semiconducting polymers. With eco-friendly materials, good electronic performance and excellent air stability, this research bridges a critical gap toward the commercialization of next-generation organic electronics.

AUTHOR INFORMATION

Corresponding Authors

Correspondence should be addressed to:

* Prof. Simon Rondeau-Gagné (srondeau@uwindsor.ca)

Author Contributions

All authors contributed to the manuscript. All authors have given approval to the final version of the manuscript.

Funding Sources

This work was supported by NSERC through a Discovery Grants (RGPIN-2017-06611) and the NSERC Green Electronics Network (GreEN) (NETGP 508526-17). S.R.-G. also acknowledge the Canada Foundation for Innovation (CFI), the Ontario Research Fund, and the University of Windsor for financial support. M. M. thanks NSERC for financial support through a Canada Postgraduate Scholarship – Doctoral. Y.W. and X.G. thank the financial support from National Science Foundation under award number DMR-2047689 for supporting the morphology characterization of the sample. This research used beamline 7.3.3 of the Advanced Light Source, which is a DOE Office of Science User Facility under contract no. DE-AC02-05CH11231. Y.W. was supported in part by an ALS Doctoral Fellowship in Residence.

Acknowledgements

The authors thank Jean-François Morin and his group (U. Laval) for MS measurements, and Max Planck Institute for Polymer Research (Germany) for the use of their facilities. This research used beamline 7.3.3 of the Advanced Light Source, a DOE Office of Science User Facility under contract DE-AC02-05CH11231.

REFERENCES

(1) Bunea, A.; Dediu, V.; Laszlo, E. A.; Pistri, F.; Iliescu, F. S.; Ionescu, O. N. E-Skin : The Dawn of a New Era of On-Body Monitoring Systems. *Micromachines* **2021**, *12*, 1091.

(2) Heo, J. S.; Eom, J.; Kim, Y.; Park, S. K. Recent Progress of Textile-Based Wearable

Electronics : And Applications. *Small* **2018**, *14*, 1703034.

(3) Schaefer, D.; Cheung, W. M. Smart Packaging: Opportunities and Challenges. *Procedia CIRP* **2023**, *72*, 1022–1027.

(4) *Organic Semiconductors in Sensor Applications*; Bernards, D. A., Owens, R. M., Malliaras, G. G., Eds.; Springer-Verlag: Berlin, 2008.

(5) Rivnay, J.; Owens, R. M.; Malliaras, G. G. The Rise of Organic Bioelectronics. *Chem. Mater.* **2014**, *26*, 679–685.

(6) Corzo, D.; Tostado-blázquez, G.; Baran, D. Flexible Electronics : Status , Challenges and Opportunities. *Front. Electron.* **2020**, *1*, 594003.

(7) Gharahcheshmeh, M. H.; Gleason, K. K. Recent Progress in Conjugated Conducting and Semiconducting Polymers for Energy Devices. *Energies* **2022**, *15*, 3661.

(8) Heeger, A. J. Semiconducting Polymers: The Third Generation. *Chem. Soc. Rev.* **2010**, *39*, 2354–2371.

(9) Lv, S.; Li, L.; Mu, Y.; Wan, X. Side-Chain Engineering as a Powerful Tool to Tune the Properties of Polymeric Field-Effect Transistors. *Polym. Rev.* **2021**, *61*, 520–552.

(10) Zhou, Y.; Li, L.; Han, Z.; Li, Q.; He, J.; Wang, Q. Self-Healing Polymers for Electronics and Energy Devices. *Chem. Rev.* **2023**, *123*, 558–612.

(11) Ocheje, M. U.; Charron, B. P.; Nyayachavadi, A.; Rondeau-Gagné, S. Stretchable Electronics: Recent Progress in the Preparation of Stretchable and Self-Healing Semiconducting Conjugated Polymers. *Flex. Print. Electron.* **2017**, *2*, 043002.

(12) Holliday, S.; Donaghey, J. E.; McCulloch, I. Advances in Charge Carrier Mobilities of Semiconducting Polymers Used in Organic Transistors. *Chem. Mater.* **2014**, *26*, 647–663.

(13) Paterson, A. F.; Singh, S.; Fallon, K. J.; Hodsden, T.; Han, Y.; Schroeder, B. C.;

Bronstein, H.; Heeney, M.; McCulloch, I.; Anthopoulos, T. D.; et al. Recent Progress in High-Mobility Organic Transistors: A Reality Check. *Adv. Mater.* **2018**, *30*, 1801079.

(14) Mooney, M.; Crep, C.; Rondeau-Gagné, S. Materials Design Strategies for Solvent-Resistant Organic Electronics. *ACS Appl. Electron. Mater.* **2022**, *4*, 5652–5663.

(15) Mooney, M.; Nyayachavadi, A.; Awada, A.; Iakovidis, E.; Wang, Y.; Chen, M. N.; Liu, Y.; Xu, J.; Chiu, Y. C.; Gu, X.; Rondeau-Gagné, S. Asymmetric Side-Chain Engineering in Semiconducting Polymers: A Platform for Greener Processing and Post-Functionalization of Organic Electronics. *Polym. Chem.* **2022**, *14*, 562–572.

(16) Hakami, A.; Srinivasan, S. S.; Biswas, P. K.; Krishnegowda, A.; Wallen, S. L.; Stefanakos, E. K. Review on Thermochromic Materials: Development, Characterization, and Applications. *J. Coatings Technol. Res.* **2022**, *19*, 377–402.

(17) Nakabayashi, K.; Takahashi, T.; Sugawara, R.; Lo, C. T.; Mori, H. Benzothiadiazole-Based Donor–Acceptor Nanoparticles with Solvatochromic and Thermoresponsive Properties. *React. Funct. Polym.* **2018**, *131*, 350–360.

(18) Yousefi, N.; Caba, C.; Hu, A.; Mooney, M.; Zhang, S.; Agostinis, A. D.; Mirhassani, M.; Ahamed, M. J.; Tong, Y.; Rondeau-Gagné, S. Building a Versatile Platform for the Detection of Protein-Protein Interactions Based on Organic Field-Effect Transistors. *ACS Appl. Electron. Mater.* **2022**, *4*, 4972–4981.

(19) Ogawa, S. *Organic Electronics Materials and Devices*; 2015.

(20) Loo, Y.; Mcculloch, I.; Editors, G. Progress and Challenges in Commercialization of Organic Electronics. *MRS Bull.* **2008**, *33*, 653–662.

(21) Luo, L.; Huang, W.; Yang, C.; Zhang, J.; Zhang, Q. Recent Advances on π-Conjugated Polymers as Active Elements in High Performance Organic Field-Effect Transistors.

Front. Phys. **2021**, *16*.

(22) Bronstein, H.; Nielsen, C. B.; Schroeder, B. C.; McCulloch, I. The Role of Chemical Design in the Performance of Organic Semiconductors. *Nat. Rev. Chem.* **2020**, *4*, 66–77.

(23) Kim, M. J.; Jung, A. R.; Lee, M.; Kim, D.; Ro, S.; Jin, S. M.; Nguyen, H. D.; Yang, J.; Lee, K. K.; Lee, E.; Kang, M. S.; Kim, H.; Choi, J. H.; Kim, B.; Cho, J. H. Structure-Property Relationships of Semiconducting Polymers for Flexible and Durable Polymer Field-Effect Transistors. *ACS Appl. Mater. Interfaces* **2017**, *9*, 40503–40515.

(24) Tao, F.; Bernasek, S. L. Understanding Odd − Even Effects in Organic Self-Assembled Monolayers. *Chem. Rev.* **2007**, *107*, 1408–1453.

(25) Morin, P.-O.; Bura, T.; Leclerc, M. Realizing the Full Potential of Conjugated Polymers: Innovation in Polymer Synthesis †. *Mater. Horizons* **2016**, *3*, 11.

(26) Teichler, A.; Perelaer, J.; Schubert, U. S. Inkjet Printing of Organic Electronics-Comparison of Deposition Techniques and State-of-the-Art Developments. *J. Mater. Chem. C* **2013**, *1*, 1910–1925.

(27) Yang, J.; Zhao, Z.; Wang, S.; Guo, Y.; Liu, Y. Insight into High-Performance Conjugated Polymers for Organic Field-Effect Transistors. *Chem* **2018**, *4*, 2748–2785.

(28) Di, C. A.; Lu, K.; Zhang, L.; Liu, Y.; Guo, Y.; Sun, X.; Wen, Y.; Yu, G.; Zhu, D. Solvent-Assisted Re-Annealing of Polymer Films for Solution-Processable Organic Field-Effect Transistors. *Adv. Mater.* **2010**, *22*, 1273–1277.

(29) Chaudhary, V.; Pandey, R. K.; Prakash, R.; Kumar, N.; Singh, A. K. Highly Aligned and Crystalline Poly(3-Hexylthiophene) Thin Films by off-Center Spin Coating for High Performance Organic Field-Effect Transistors. *Synth. Met.* **2019**, *258*, 116221.

(30) Mooney, M.; Wang, Y.; Nyayachavadi, A.; Zhang, S.; Gu, X.; Rondeau-Gagné, S.

Enhancing the Solubility of Semiconducting Polymers in Eco-Friendly Solvents with Carbohydrate-Containing Side Chains. *ACS Appl. Mater. Interfaces* **2021**, *13*, 25175–25185.

(31) Mooney, M.; Wang, Y.; Iakovidis, E.; Gu, X.; Rondeau-Gagné, S. Carbohydrate-Containing Conjugated Polymers: Solvent-Resistant Materials for Greener Organic Electronics. *ACS Appl. Electron. Mater.* **2021**, *4*, 1381–1390.

(32) Yu, H.; Park, K. H.; Song, I.; Kim, M. J.; Kim, Y. H.; Oh, J. H. Effect of the Alkyl Spacer Length on the Electrical Performance of Diketopyrrolopyrrole-Thiophene Vinylene Thiophene Polymer Semiconductors. *J. Mater. Chem. C* **2015**, *3*, 11697–11704.

(33) Lei, T.; Cao, Y.; Zhou, X.; Peng, Y.; Bian, J.; Pei, J. Systematic Investigation of Isoindigo-Based Polymeric Field-Effect Transistors: Design Strategy and Impact of Polymer Symmetry and Backbone Curvature. *Chem. Mater.* **2012**, *24*, 1762–1770.

(34) Schroeder, B. C.; Kurosawa, T.; Fu, T.; Chiu, Y. C.; Mun, J.; Wang, G. J. N.; Gu, X.; Shaw, L.; Kneller, J. W. E.; Kreouzis, T.; Toney, M. F.; Bao, Z. Taming Charge Transport in Semiconducting Polymers with Branched Alkyl Side Chains. *Adv. Funct. Mater.* **2017**, *27*.

(35) Ocheje, M. U.; Charron, B. P.; Cheng, Y. H.; Chuang, C. H.; Soldera, A.; Chiu, Y. C.; Rondeau-Gagné, S. Amide-Containing Alkyl Chains in Conjugated Polymers: Effect on Self-Assembly and Electronic Properties. *Macromolecules* **2018**, *51*, 1336–1344.

(36) Yuan, G. C.; Xu, Z.; Gong, C.; Cai, Q. J.; Lu, Z. S.; Shi, J. S.; Zhang, F. J.; Zhao, S. L.; Xu, N.; Li, C. M. High Performance Organic Thin Film Transistor with Phenyltrimethoxysilane- Modified Dielectrics. *Appl. Phys. Lett.* **2009**, *94*.

(37) Randell, N. M.; Kelly, T. L. Recent Advances in Isoindigo-Inspired Organic

Semiconductors. *Chem. Rec.* **2019**, *19*, 973–988.

(38) Luo, N.; Ren, P.; Feng, Y.; Shao, X.; Zhang, H. L.; Liu, Z. Side-Chain Engineering of Conjugated Polymers for High-Performance Organic Field-Effect Transistors. *J. Phys. Chem. Lett.* **2022**, *13*, 1131–1146.

(39) Yu, H.; Park, K. H.; Song, I.; Kim, M.-J.; Kim, Y.-H.; Oh, J. H. Effect of the Alkyl Spacer Length on the Electrical Performance of Diketopyrrolopyrrole-Thiophene Vinylene Thiophene Polymer Semiconductors. *J. Mater. Chem. C* **2015**, *3*, 11697–11704.

(40) Duarte, D.; Sharma, D.; Cobb, B.; Dodabalapur, A. Charge Transport and Trapping in Organic Field Effect Transistors Exposed to Polar Analytes. *Appl. Phys. Lett.* **2011**, *98*.

(41) Kim, S.; Yoo, H.; Choi, J. Effects of Charge Traps on Hysteresis in Organic Field-Effect Transistors and Their Charge Trap Cause Analysis through Causal Inference Techniques. *Sensors* **2023**, *23*.

(42) Saito, M.; Koganezawa, T.; Osaka, I. Understanding Comparable Charge Transport Between Edge-on and Face-on Polymers in a Thiazolothiazole Polymer System. *Appl. Polym. Mater.* **2019**, *1*, 1257–1262.

(43) Griggs, S.; Marks, A.; Bristow, H.; McCulloch, I. N-Type Organic Semiconducting Polymers: Stability Limitations, Design Considerations and Applications. *J. Mater. Chem. C* **2021**, *9*, 8099–8128.

(44) Dobryden, I.; Korolkov, V. V.; Lemaur, V.; Waldrip, M.; Un, H. I.; Simatos, D.; Spalek, L. J.; Jurchescu, O. D.; Olivier, Y.; Claesson, P. M.; Venkateshvaran, D. Dynamic Self-Stabilization in the Electronic and Nanomechanical Properties of an Organic Polymer Semiconductor. *Nat. Commun.* **2022**, *13*, 1–11.

(45) Lüssem, B.; Keum, C. M.; Kasemann, D.; Naab, B.; Bao, Z.; Leo, K. Doped Organic

Transistors. *Chem. Rev.* **2016**, *116*, 13714–13751.

(46) Abdou, M. S. A.; Orfino, F. P.; Son, Y.; Holdcroft, S. Interaction of Oxygen with Conjugated Polymers: Charge Transfer Complex Formation with Poly(3-Alkylthiophenes). *J. Am. Chem. Soc.* **1997**, *119*, 4518–4524.

(47) Lu, C. K.; Meng, H. F. Hole Doping by Molecular Oxygen in Organic Semiconductors: Band-Structure Calculations. *Phys. Rev. B - Condens. Matter Mater. Phys.* **2007**, *75*, 2–7.

(48) Hines, D. R.; Ballarotto, V. W.; Williams, E. D.; Shao, Y.; Solin, S. A. Transfer Printing Methods for the Fabrication of Flexible Organic Electronics. *J. Appl. Phys.* **2007**, *101*, 024503.

(49) Nayak, P. K.; Rosenberg, R.; Barnea-Nehoshtan, L.; Cahen, D. O2 and Organic Semiconductors: Electronic Effects. *Org. Electron.* **2013**, *14*, 966–972.

(50) Lamport, Z. A.; Haneef, H. F.; Anand, S.; Waldrip, M.; Jurchescu, O. D. Organic Field-Effect Transistors: Materials, Structure and Operation. *J. Appl. Phys.* **2018**, *124*, 071101.

(51) Ante, F.; Kälblein, D.; Zschieschang, U.; Canzler, T. W.; Werner, A.; Takimiya, K.; Ikeda, M.; Sekitani, T.; Someya, T.; Klauk, H. Contact Doping and Ultrathin Gate Dielectrics for Nanoscale Organic Thin-Film Transistors. *Small* **2011**, *7*, 1186–1191.

(52) Kraft, U.; Anthony, J. E.; Ripaud, E.; Loth, M. A.; Weber, E.; Klauk, H. Low-Voltage Organic Transistors Based on Tetraceno[2,3-b]Thiophene: Contact Resistance and Air Stability. *Chem. Mater.* **2015**, *27*, 998–1004.

(53) Kraft, U.; Takimiya, K.; Kang, M. J.; Rödel, R.; Letzkus, F.; Burghartz, J. N.; Weber, E.; Klauk, H. Detailed Analysis and Contact Properties of Low-Voltage Organic Thin-Film Transistors Based on Dinaphtho[2,3-b:2′,3′-f]Thieno[3,2-b]Thiophene (DNTT) and Its Didecyl and Diphenyl Derivatives. *Org. Electron.* **2016**, *35*, 33–40.